Title

A Mononuclear Iron-Dependent Methyltransferase Catalyzes Initial Steps in Assembly of the Apratoxin A Polyketide Starter Unit

Journal

ACS Chemical Biology, 12(12)

ISSN

1554-8929

Authors

Skiba, Meredith A
Sikkema, Andrew P
Moss, Nathan A
et al.

Publication Date

2017-12-15

DOI

10.1021/acschembio.7b00746

Peer reviewed

HHS Public Access

Author manuscript

ACS Chem Biol. Author manuscript; available in PMC 2018 December 15.

Published in final edited form as:

ACS Chem Biol. 2017 December 15; 12(12): 3039–3048. doi:10.1021/acschembio.7b00746.

A Mononuclear Iron-Dependent Methyltransferase Catalyzes Initial Steps in Assembly of the Apratoxin A Polyketide Starter Unit

Meredith A. Skiba[a,b], **Andrew P. Sikkema**[a,b], **Nathan A. Moss**[c], **Collin L. Tran**[a], **Rebecca M. Sturgis**[a], **Lena Gerwick**[c], **William H. Gerwick**[c,d], **David H. Sherman**[a,e,f,g], and **Janet L. Smith**[a,b,*]

[a]Life Sciences Institute, University of Michigan, Ann Arbor, MI 48109

[b]Department of Biological Chemistry, University of Michigan, Ann Arbor MI, 48109

[c]Center for Marine Biotechnology and Biomedicine, Scripps Institution of Oceanography, University of California, San Diego, La Jolla, CA 92093

[d]Skaggs School of Pharmacy and Pharmaceutical Sciences, University of California, San Diego, La Jolla, CA 92093

[e]Department of Medicinal Chemistry, University of Michigan, Ann Arbor, MI 48109

[f]Department of Chemistry, University of Michigan, Ann Arbor, MI 48109

[g]Department of Microbiology and Immunology, University of Michigan, Ann Arbor, MI 48109

Abstract

Natural product biosynthetic pathways contain a plethora of enzymatic tools to carry out difficult biosynthetic transformations. Here we discover an unusual mononuclear iron-dependent methyltransferase that acts in the initiation steps of apratoxin A biosynthesis (AprA MT1). Fe^{3+}-replete AprA MT1 catalyzes one or two methyl transfer reactions on the substrate malonyl-ACP (acyl carrier protein), whereas Co^{2+}, Fe^{2+}, Mn^{2+} and Ni^{2+} support only a single methyl transfer. MT1 homologs exist within the "GNAT" (GCN5-related *N*-acetyltransferase) loading modules of several modular biosynthetic pathways with propionyl, isobutyryl or pivaloyl starter units. GNAT domains are thought to catalyze decarboxylation of malonyl-CoA and acetyl transfer to a carrier protein. In AprA the GNAT domain lacks both decarboxylation and acyl transfer activity. A crystal structure of the AprA MT1-GNAT didomain with bound Mn^{2+}, malonate and the methyl donor *S*-adenosylmethionine (SAM) reveals that the malonyl substrate is a bidentate metal ligand, indicating that the metal acts as a Lewis acid to promote methylation of the malonyl α-carbon. The GNAT domain is truncated relative to functional homologs. These results afford an expanded understanding of MT1-GNAT structure and activity, and permit the functional annotation of

*To whom correspondence should be addressed JanetSmith@umich.edu.

Accession Codes. The atomic coordinates and structure factors have been deposited in the Protein Data Bank (PDB ID codes 6B39 (AprA MT1-ΨGNAT SAH bound), 6B3A (AprA MT1-ΨGNAT Mn^{2+} and SAM bound), and 6B3B (AprA MT1-ΨGNAT malonate, Mn^{2+} and SAM bound).

homologous GNAT loading modules both with and without methyltransferases, additionally revealing their rapid evolutionary adaptation in different biosynthetic contexts.

INTRODUCTION

Prokaryotic secondary metabolite biosynthetic pathways use an assortment of enzymatic tools to synthesize some of the most elegant and chemically complex molecules found in nature. Polyketide metabolites are mostly synthesized through the successive condensation of malonyl or methylmalonyl coenzyme A (CoA) extender units in a manner similar to fatty acid biosynthesis. In type I modular polyketide synthase (PKS) systems, each extension step starts with acyltransferase (AT) selection of a specific carboxyacyl-CoA for transfer to the phosphopantetheine (Ppant) cofactor of the acyl carrier protein (ACP) domain within the module. This is followed by decarboxylative condensation with the upstream intermediate in the ketosynthase (KS) domain, and then by optional modifications by ketoreductase, dehydratase, enoylreductase or methyltransferase (MT) domains in the module, or external enzymes encoded in the gene cluster [1]. In this manner PKS systems synthesize a variety of essential pharmaceuticals, such as the anthelmintic avermectin, immunosuppressant rapamycin, and antibiotic erythromycin, using a common set of enzymes [2-4]. In some cases, PKS modules are interspersed with non-ribosomal peptide synthetase (NRPS) modules, which incorporate amino acid building blocks into the linear product.

Modular PKS systems initiate biosynthesis in a “loading module” by transfer of a specific acyl group to the loading ACP. Several mechanisms of pathway initiation have been described; frequently, a loading acyltransferase (AT_L) primes the ACP with an acyl group such as acetyl-, malonyl-, or methylmalonyl-CoA. An α-carboxylated acyl group can be decarboxylated by a non-extending ketosynthase domain [5]. In other cases, the loading modules select chemically diverse starter units derived from amino acids, cyclohexanecarboxylic acids, fatty acids, or branched chain CoAs [5, 6]. For example, isobutyryl-CoA, methylbutyryl-CoA, and isovaleryl-CoA, derived from the catabolism of valine, leucine, and isoleucine through a branched chain α-keto acid dehydrogenase (BCDH) complex, are the starter units in the biosynthesis of virginiamycin, avermectin and myxothiazol, respectively [7-10]. An AT_L directly primes the ACP with the branched-chain acyl group in these pathways [2, 11, 12].

We previously reported the discovery and characterization of the GNAT loading module family (Figure 1). The CurA loading module [13] initiates biosynthesis of the anti-cancer cyanobacterial compound curacin A[14]. Although the GNAT superfamily generally includes CoA-dependent *N*-acetyltransferases [15, 16], the CurA GNAT is a remarkable bifunctional enzyme that decarboxylates malonyl-CoA to acetyl-CoA and catalyzes *S*-acetyltransfer to an associated ACP [13]. Clues to the evolutionary origin of the CurA GNAT decarboxylase activity came from the subsequent discovery that malonyl-CoA decarboxylase (MCD) is a GNAT superfamily member [17]. MCD, which is conserved from bacteria to humans, catalyzes only decarboxylation. Thus, the GNAT superfamily may be better described as a “CoA binding” family, as members have a common mode of CoA binding and may catalyze acyltransfer, decarboxylation or both.

GNAT loading modules in biosynthetic pathways for natural products that contain branched-chain starter units also include a putative methyltransferase domain (MT1), which precedes the GNAT domain in the module (Figure 1a, 1b, 1c) [18, 19]. This path to incorporation of branched-chain starter units was identified recently in the annotation of gene clusters for biosynthesis of gephyronic acid (Gph) [18] and apratoxin A (Apr) [20, 21], a Sec61 inhibitor [22, 23]. Based on the natural product structures, the AprA loading module installs a pivaloyl group, whereas GphF introduces an isobutyryl group into gephyronic acid (Figure 1a, 1b). Isotopic labeling of the gephyronic acid producer *Cystobacter violaceus* with ^{13}C-methyl-L-methionine demonstrated that the isobutyryl starter group is derived from *S*-adenosylmethionine (SAM) and not from valine, likely via GphF MT1 [18]. The MT1-containing loading modules also include a mysterious ~150-residue N-terminal "adaptor region" (AR), which has no detectable homology to proteins of known structure or function. The AR domain of CurA (Figure 1f) enhanced, but was not essential to, the GNAT *S*-acyltransfer activity [13]. Pivaloyl-producing modules, such as AprA, include an additional methyltransferase (MT2) following the GNAT (Figure 1a) [20]. The MT1 sequences are highly conserved, but are distantly related to methyltransferases of known structure and to MT2.

Here we describe initial steps in the production of branched-chain polyketide starter units by GNAT loading modules. Through structural and biochemical characterization of AprA MT1, we discovered an unusual mononuclear iron-dependent methyltransferase, which catalyzes two methyl transfer reactions to produce dimethylmalonyl-ACP. Methylmalonyl- or dimethylmalonyl-ACP produced by MT1 homologs can be further decarboxylated by GNAT to yield propionyl or isobutyryl starter units. In pivalate-producing modules, such as AprA, the GNAT is truncated and not catalytically active. Characterization of AprA MT1 resolves the functional annotation of GNAT loading modules from several biosynthetic pathways, including gephyronic acid [18], myxovirescin [24], saxitoxin [19] and bryostatin [25].

RESULTS AND DISCUSSION

Bioinformatic analysis of MT1-GNAT loading modules

The AprA amino acid sequence was used to identify several homologs of AR-MT1-GNAT in annotated and unannotated secondary metabolite biosynthetic pathways in proteobacteria, cyanobacteria, dinoflagellates, firmicutes, and planctomycetes. The homologous sequences from pathways with characterized natural products represent loading modules that incorporate starter units larger than acetate (propionate, isobutyrate), which could be derived from the decarboxylation of methylmalonyl- or dimethylmalonyl-CoA/ACP or from methylation of acetyl- or propionyl-CoA/ACP (Figure 1a, 1b, 1c). Our search identified an unannotated MT domain in the myxovirescin biosynthetic pathway where TaI module 1 contains an AR-MT1-GNAT tridomain (Figure 1c) that could generate a propionyl starter unit for synthesis of the myxovirescin C3-hydroxyvaleryl moiety, consistent with ^{13}C labeling studies [24]. Another variant occurs in the rhizoxin pathway, which incorporates an unbranched acetyl starter unit despite the AR-MT1-GNAT loading module architecture (Figure 1d) [26]. However, the RhiA MT1 sequence lacks the characteristic SAM-binding motifs, indicating that it is nonfunctional (Supplementary Figure 1). We also identified several AR-MT1-GNAT loading-module variants that lack AR, MT1 or both [MT1-GNAT-

ACP (Figure 1e), AR-GNAT-ACP (Figure 1f), GNAT-ACP (Figure 1g)]. and have predicted acetyl starter units. We conclude from the sequence analysis that AR-MT1-GNAT loading modules produce starter units larger than acetyl by SAM-dependent methyl transfer via the MT1, and that both AR and a functional MT1 are required for the biosynthesis of *C*-methylated acetyl starter units.

AprA, the pivaloyl-producing loading module in apratoxin biosynthesis, contains a second MT (MT2) following the GNAT (Figure 1a) [20]. Among several homologous sequences having both MT1 and MT2 domains, only AprA and BryX are from pathways with natural products of known structure. The *bryX* gene is a poorly characterized element of the gene cluster for bryostatin [25], a protein kinase C modulator [27]. The AR-MT1-GNAT-MT2-ACP domain architecture of BryX is consistent with several isolated bryostatins that contain pivaloyl groups [25], leading to the prediction that MT2 is needed for a third methyl transfer in both apratoxin and bryostatin biosynthesis.

AprA AR-MT1-GNAT Structure

In order to understand the function of the common AR-MT1-GNAT loading module, we sought a stable AprA fragment for biochemical and structural studies. By screening several fragments for solubility, we identified a stable tridomain (residues 2–629), and solved a 2.4-Å crystal structure by single-wavelength anomalous diffraction (SAD) from the selenomethionyl protein (Figure 2a, Supplementary Table 1). Crystal growth required two serendipitous amino acid substitutions (S274I, Q528P) that were introduced during cloning and are located in crystal contacts. AprA AR-MT-GNAT is monomeric in crystals and in solution as determined by gel filtration chromatography. The MT1 domain (residues 241–505) has a typical class I MT fold and forms the SAM-binding core. The crystallization solution included SAM, but crystals contained the hydrolysis product *S*-adenosylhomocysteine (SAH) with clear density for the adenosine portion and poorly ordered homocysteine (Figure 3a, Supplementary Figure 3a). The mysterious AR domain (residues 1–227) is a large helical lid capping the MT1 core. As MTs typically include a lid domain, hereafter we refer to the AR-MT1 didomain as MT1. The substantial sequence conservation within the lid consists of hydrophobic side chains that pack in the domain interior. A highly conserved 13-residue linker (residues 228–240) connects the MT1 lid and core, and is adjacent to the SAM binding site, but was disordered and lacked electron density.

The AprA GNAT (residues 505–621) is closely associated with MT1, with only four amino acids between the last β-strand of the MT1 core and the first β-strand of the GNAT. The GNAT packs against a hydrophobic surface of MT1 helix 22, perhaps explaining why attempts to produce MT1 without GNAT resulted in insoluble protein. Interestingly, the AprA and CurA GNAT domains are highly similar for the first ~90 amino acids, after which the structures and sequences diverge abruptly (Supplementary Figure 2). AprA GNAT is ~70 amino acids shorter than the CurA GNAT, specifically lacking the substrate binding tunnel and the His and Thr residues critical for decarboxylation (Supplementary Figure 4a) [13]. Attempts to produce a longer MT1-GNAT resulted in insoluble protein. Based on the structure superposition and sequence alignment, we conclude that the AprA GNAT is not a

decarboxylase, and moreover, appears to be a remnant protein lacking a catalytic role and can be reclassified as a pseudo-GNAT (ΨGNAT).

Structural homology of MT1

Among all entries in the structure database, the AprA MT1 core domain structure is most similar to the two PKS *C*-methyltransferases, the CurJ MT domain (PDB 5THY, 13% sequence identity, RMSD 3.0 Å for 98 core Cα atoms) (Supplementary Figure 4) and the fungal-derived citrinin MT domain (5MPT, 13% identity, RMSD 2.0 Å for 112 Cα atoms), which methylate the β-keto intermediate produced by a KS condensation reaction [28, 29]. Another homolog is MppJ (4KIG, 15% identity, RMSD 2.9 Å for 121 Cα atoms), a methyltransferase from the mannopeptimycin biosynthetic pathway in *Streptomyces hygroscopicus*. MppJ uses a mononuclear iron, coordinated by two histidines and two waters bridged to an aspartic acid, to facilitate *C*-methylation at the benzylic position of phenylpyruvate [30]. In the AprA MT1-ΨGNAT structure, His369 and His456 near the SAM binding site appeared to be positioned perfectly to serve as metal ligands similar to those in MppJ.

AprA MT1 catalyzes iron-dependent methyltransfer

AprA MT1-ΨGNAT was tested for SAM-dependent methyl transfer activity on a variety of acyl-ACPs (malonyl, methylmalonyl, acetyl, propionyl, isobutyryl) using excised AprA ACP. Reaction mixtures were monitored for product formation by mass spectrometry (MS) detection of ACP species. The phosphopantetheine (Ppant) ejection assay, which dissociates the Ppant fragment from the ACP phosphoserine linkage during ionization, was used for quantification based upon the relative abundance of Ppant species [31, 32]. No activity was observed for any acyl-ACP substrate tested. Inspired by the metal dependence of MppJ, we screened a panel of biologically relevant metals for their effect on activity (Figure 4, Supplementary Figure 5, 6). AprA MT1-ΨGNAT catalyzed methylation of malonyl-ACP to methylmalonyl-ACP in the presence of Fe^{2+}, Mn^{2+}, Co^{2+}, and Ni^{2+}. With added Fe^{2+} under aerobic conditions, MT1-ΨGNAT had a nearly three-fold higher activity than with the other active metals. Additionally aerobic reconstitution with Fe^{2+} yielded significant quantities of dimethylmalonyl-ACP (Figure 4b). As Fe^{2+} readily oxidizes to Fe^{3+} in aerobic environments and as activity is greatly reduced under anaerobic conditions, we infer that Fe^{3+} is the active metal.

AprA MT1-ΨGNAT also methylated malonyl- and methylmalonyl-CoA, but had twofold lower activity with CoA-linked than with ACP-linked substrates under similar reaction conditions (Supplementary Figure 7). Like AprA MT1, GphF MT1 also catalyzed Mn- and SAM-dependent methylation of malonyl-ACP, and produced both methylmalonyl- and dimethylmalonyl-ACP with Fe^{3+} (Supplementary Figure 8). This GphF MT1 activity is consistent with the predicted isobutyryl starter unit of gephyronic acid biosynthesis [18].

In contrast to the methylation of malonyl-ACP, we detected no AprA MT1 methylation of acetyl, propionyl, or isobutyryl-ACP in the presence of Fe^{3+} (Supplementary Figure 9a, 9b, 9c). There was also no detectable decarboxylation of malonyl-, methylmalonyl- or dimethylmalonyl-ACP in mass spectra of intact ACP species (Supplementary Figure 5b), nor

any enzyme-catalyzed acyl transfer from malonyl-CoA or methylmalonyl-CoA to the AprA ACP (Supplementary Figure 9d, 9e), confirming that AprA ΨGNAT has no catalytic activity.

Metal binding triggers tunnel formation

The metal in MT1 is labile; AprA MT1 purified without bound metal, and after reconstitution, did not retain iron during size exclusion chromatography. This property contrasts with MppJ, which co-purified with Fe^{3+} [30]. Metal addition blocked AprA MT1-ΨGNAT crystallization in the previously identified conditions, but new conditions with 5 mM $MnCl_2$ resulted in a new crystal form and a 1.8-Å structure of AprA MT1-ΨGNAT S274I/Q528P (Figure 2b and Supplementary Table 1). Mn^{2+} is bound ~6 Å from the SAM methyl donor. The octahedral coordination sphere consists of three water ligands and three protein ligands (Figure 3b), including Gln461 and the predicted His369 and His456. These three ligands are conserved in MT1 homologs (Supplementary Figure 1), the only exceptions being a few cases of Gln in place of His456. No charged ligand resides in the first coordination shell, but one water ligand is bridged to Asp370. A D370N substitution resulted in a slight decrease in activity (Figure 6).

Metal binding induced a substantial reorganization of the active site, especially in the conserved linker between the MT1 lid and core (residues 228–240), which was disordered in the metal-free structure. Amino acids 228–251 form a helix (helix 14) and loop that extend over the metal center and SAM binding site, and create a tunnel between the lid and core (Figure 2b, 3b). Surprisingly, intact SAM was bound in the Mn^{2+} complex, suggesting that the fully formed active site protects SAM from hydrolysis. In contrast to the metal-free structure, the methionine portion of SAM was well ordered (Figure 3b, Supplementary Figure 3b). The SAM carboxylate is hydrogen bonded with the His249 imidazole, which points into the active site between SAM and Mn^{2+} (Figure 5). A H249A substitution abolished activity with malonyl-ACP substrates (Figure 6). Second-shell interactions at the metal center are also important to catalysis. The Gln461 and His369 metal ligands are positioned by conserved residues Tyr206 in the lid domain, and Glu431 in the core. A Y206F substitution eliminated activity (Figure 6). His462 lies on a loop following His456 and Gln461, and appears to stabilize these ligands through hydrogen bonds with adjacent loops. Substitution at His462 resulted in a twofold decrease in activity (Figure 6).

Substrate Binding and Catalysis

In order to understand how the metal center promotes catalysis, we obtained a 1.85-Å structure for an MT1-ΨGNAT complex with Mn^{2+}, SAM and malonate (Figure 3c, 5, Supplementary Table 1). Malonate binds directly to Mn^{2+} as a bidentate ligand in which one coordination bond from each carboxylate displaces a water ligand. One malonate carboxylate is clearly in the position of the terminal group of malonyl-ACP as it forms three hydrogen bonds with conserved amino acids: Tyr206, Asn241 and Gln461, which are in turn positioned by an extensive hydrogen bond network with other conserved residues [Ser205 in the lid, and Glu233 and Arg238 in the re-ordered lid-core connector, (Figure 5)]. Methyl transfer activity was abolished by substitution of Asn241 or any connector amino acids in the hydrogen bond network, including His235 (Figure 6). The second malonate carboxylate

is well positioned to form the thioester with the ACP Ppant as it lacks hydrogen bonds to the protein and the non-coordinated oxygen points into the tunnel between the lid and core. Like the metal center, the malonate has no direct contact with charged amino acids. This should enhance the ionic interaction of malonate and metal, and the ability of the metal to promote methyl transfer.

Metal-dependent MTs typically require Ca^{2+} or Mg^{2+}, which functions to position the substrate for methyl addition and proton abstraction from a relatively acidic oxygen [33-35]. Compared to a hydroxy oxygen, the weak acidity of the α-carbon renders malonyl-ACP a far more challenging methylation target. The mannopeptimycin methyltransferase MppJ, which methylates phenylpyruvate at a benzylic carbon of similarly weak acidity [30], provides a direct precedent for the Fe^{3+}-dependence of the AprA MT1.

We propose that the metal facilitates catalysis by acting as a Lewis acid to lower the pKa of the malonyl or methylmalonyl α-carbon, leading to deprotonation, enolate formation and attack of the SAM methyl (Figure 7), similar to the mechanism proposed for Co^{2+}-dependent epimerization of methylmalonyl-CoA [36]. The positions of malonate and SAM indicate that the product of the first methyl transfer is (*S*)-methylmalonyl-ACP (Figure 3c, 5). The malonyl α-carbon is 6.8 Å from the SAM methyl, suggesting that further closure of the MT1 active site occurs prior to methyl transfer. Tyr455 and Ser245 are the only amino acids in the active site positioned (5.0 Å and 4.1 Å, respectively) to accept an α-proton. Interestingly, a Y455F substitution and an S245A substitution abrogated the second methyl transfer but not the first (Figure 6b). This raises the possibility that one of these side chains accepts the α(*R*)-proton in the second methyl transfer reaction and that another base accepts the α(*S*)-proton prior to the first methyl transfer. The only candidate for an α(*S*)-proton acceptor is the water molecule that bridges Asp370 and the metal (3.5 Å from the malonyl α-carbon).

The few examples of mononuclear iron as a Lewis acid include nitrile hydratase and the MppJ MT, which both employ Fe^{3+} [30, 37, 38]. Ferric iron supports AprA MT1 catalysis, as our assays were performed in an aerobic environment over several hours and activity was diminished under anaerobic conditions (Figure 4). Although AprA can perform monomethylation with Co^{2+}, Fe^{2+}, Mn^{2+}, and Ni^{2+}, dimethylation is dependent on Fe^{3+} as a co-factor (Figure 4b). We infer that the second AprA MT1 methylation is more energetically demanding than the first due to the difference in pKa values reported for methyl ester forms of malonate (15.9) and methylmalonate (18.0) [39]. Ferric iron may be uniquely capable of facilitating the removal of the second proton for the formation of dimethylmalonyl-ACP, as it is a stronger Lewis acid than Co^{2+}, Fe^{2+}, Mn^{2+} and Ni^{2+}. Despite the biosynthetic challenge, nature has evolved other approaches to generate the dimethylmalonyl biosynthetic subunit, as two non-metal dependent PKS extension module *C*-MTs have also been reported to produce dimethylmalonyl-ACP [40-42].

Ppant Modeling

We modeled malonyl-Ppant into the AprA MT1 structure based on the outermost carboxylate of bound malonate (Figure 8a). The tunnel width and length are well matched for threading Ppant to deliver malonyl to the active site. The Ppant could interact with

conserved tunnel residues Gln248 and Arg496, which coordinates a glycerol molecule from the crystallization solution. Although Arg496 is 10 Å from the metal center, an Ala substitution abolished activity (Figure 6a), suggesting that Ppant interactions within the tunnel are essential for activity. The proposed Ppant tunnel entrance is surrounded by positively charged amino acids (Arg196, Lys251, Lys290). R196E, K251E and K490E variants yielded no activity (Figure 6a). A complementary negatively charged surface is adjacent to the Ppant attachment site (Ser1093) in a homology model for AprA ACP. This charge complementarity may facilitate the interaction between AprA MT1 and ACP (Figure 8b, 8c). Ppant binding in the tunnel is compatible with exchange of SAH for SAM through the opposite end of the tunnel, facilitating the second methylation reaction prior to disengagement of methylmalonyl-ACP (Figure 8a). Evidence that two methylations occur prior to dissociation of ACP from the enzyme comes from the nearly identical accumulation rates of methylmalonyl-ACP and dimethylmalonyl-ACP in a reaction starting with malonyl-ACP, indicating no initial accumulation of the singly methylated product, methylmalonyl-ACP (Supplementary Figure 6a).

Relation of AprA MT1 to other PKS MTs

Of the several hundred MT structures in the structure database, AprA MT1 most closely resembles the MTs from PKS extension steps [28, 29]. All class I SAM-dependent MTs are thought to have a common ancestor, but the superfamily has several highly diverged branches. AprA shares several features with the PKS extension module MTs (Supplementary Figure 4b, 4c) [28], including a lid-interacting insertion between β-strands five and six of the core. The lid domains are topologically similar at the N-termini, but the AprA MT1 lid (formerly known as AR) is much larger due to a C-terminal extension. We previously showed that conserved His and Glu amino acids are essential to methyl transfer by the CurJ extension-module MT, and proposed that the His imidazole is the catalytic base that accepts a proton from the α-carbon of the β-ketoacyl-ACP substrate [28]. By structure superposition, the critical His and Glu of extension-module MTs correspond to AprA MT1 His369 and Glu431, which are also conserved in GNAT loading modules (Supplementary Figure 4d, 4e). His369 is a metal ligand, and Glu431 is hydrogen bonded to the second imidazole nitrogen of His369, exactly as in the CurJ MT. Interestingly, CurJ MT acts on acetoacetyl-ACP, but has no activity with malonyl-ACP, even with the addition of iron (Supplementary Figure 9f), and lacks the other metal ligands (His456 and Gln461). Thus, it appears that an ancestral extension-step MT acquired a metal center as it adapted from a-methylation of β-ketoacyl-ACP to the more energetically demanding α-methylation of β-carboxyacyl-ACP.

The dual entrances to the active site are a major difference between AprA MT1 and both the PKS extension *C*-MTs, which have a single active-site entrance. In extension module *C*-MTs, the Ppant tunnel entrance is blocked by an N-terminal helix [28]. Thus, it appears that AprA MT1 has specifically evolved two active site entrances, which may be essential to performing the dimethylation reaction.

Functional Annotation of GNAT Loading Modules

The discovery of iron-dependent methylation of malonyl-ACP by AprA MT1 and homologs permits the functional annotation of branched-chain acyl group production by GNAT loading modules for several PKS pathways, including bryostatin (pivalate), gephyronic acid (isobutyryl), myxovirescin (propionyl) and saxitoxin (propionyl). The loading modules that generate pivaloyl-ACP, AprA and BryX, have an MT1-ΨGNAT-MT2-ACP architecture, as the ΨGNAT lacks the His and Thr/Ser residues required for decarboxylation and also the substrate tunnel for malonyl-CoA binding [13]. Consistent with the structure and sequence we observed no decarboxylation of malonyl-, methylmalonyl- or dimethylmalonyl-ACP in assays of AprA MT1-ΨGNAT. Additionally, no malonyl- or methylmalonyl-CoA transfer to the ACP was observed by the ΨGNAT (Supplementary Figure 9d, 9e). Thus, for the MT1-ΨGNAT-MT2-ACP loading modules AprA and BryX, the identity of the enzyme responsible for activating and catalyzing transfer of the malonyl group onto the ACP is unknown, as is the identity of the corresponding decarboxylase.

In modules containing MT1-GNAT-ACP, such as GphF, TaI and SxtA (Figure 1b, 1c), MT1 catalyzes one or two methyl transfer reactions on malonyl-ACP. No evident sequence motifs or structural features distinguish monomethylating and dimethylating MT1 enzymes. The methylmalonyl- or dimethylmalonyl-ACP product should be decarboxylated by GNAT to yield propionyl- or isobutyryl-ACP starter units, as all GNAT domains in MT1-GNAT-ACP modules contain the His and Thr/Ser side chains required for decarboxylation [13]. Unlike the CurA GNAT, the GNAT of pathways with branched-chain starter units should not catalyze decarboxylation of malonyl-CoA. These GNATs may transfer malonyl from CoA to ACP to initiate starter unit biosynthesis, however this would require the ACP-bound substrate to occupy the GNAT active site both before and after MT1 methylation. This process could additionally lead to aberrant product formation through premature decarboxylation of malonyl-ACP. Therefore for propionyl- or isobutyryl-ACP production, we reason that an enzyme outside the module transfers malonyl to the ACP. For pathways with *in trans* acyltransferases (AT), one or more loading enzymes are encoded in the gene cluster. For pathways with *in cis* ATs, the loading enzyme is unknown, but may be a malonyl acyltransferase from fatty acid biosynthesis, as observed in other polyketide pathways [43-45].

Evolution of GNAT Loading Modules

The extant GNAT loading modules are remarkable examples of PKS evolution in action. AR-MT1-GNAT-ACP modules are capable of synthesizing propionyl or isobutyryl starter units. In order to form a pivaloyl starter unit, a second methyltransferase (MT2), which is most similar to PKS extension-step *C*-MTs, is inserted into the module. However, it appears that the decarboxylation and acyltransfer functions of GNAT were lost in pivaloyl-producing modules, yielding a ΨGNAT. GNAT loading modules that introduce an acetyl starter unit are presumed to function like the CurA GNAT by decarboxylation of malonyl-CoA and acetyl transfer to the ACP. Several of these loading modules retain vestiges of an MT ancestor. For example, the MT1 core domain was lost from the curacin A loading module (Figure 1f) but the AR, which we now know is a remarkably large MT1 lid, was retained and enhances, but is not required for, GNAT loading activity[13]. In contrast, GNAT loading modules from the batumin (Bat) and nosperin (Nsp) pathways have lost the AR and contain only $MT1_{core}$-

GNAT-ACP (Figure 1e) [46, 47]. The rhizoxin GNAT loading module has homologs of all domains, but the MT1 appears to be non-functional (Figure 1d). Finally, minimal GNAT loading modules in the bongkrekic acid (Bon), onnamide A (Onn), and pederin (Ped) pathways contain only GNAT and ACP (Figure 1g) [48-50].

In conclusion, we have characterized an unusual Fe^{3+}- and SAM-dependent methyltransferase involved in the production of branched polyketide starter units. Although related to other PKS MTs, the MTs of GNAT loading modules have evolved to have two active site entrances to facilitate dimethylation. A crystal structure in complex with malonate, a substrate mimic, reveals an elegant conserved hydrogen bond network responsible for positioning the substrate. Functional and structural characterization of the AprA MT1 provides key insights to enable a more robust annotation of GNAT loading modules found in diverse microorganisms.

METHODS

Construct Design, Protein Expression, and Purification

Full-length *aprA* was amplified from an apratoxin fosmid library [20] and cloned into pMCSG7 [51] via ligation independent cloning (LIC) to create pAPS1. The region encoding MT1-ΨGNAT (AprA residues 2–629) was subcloned from pAPS1 to create pMAS286. This plasmid contains two PCR-induced missense mutations (S274I and Q528P), which were corrected using the QuickChange protocol (Stratagene) to create pMAS354. All *aprA* site-directed mutants were created from pMAS286. The region encoding AprA ΨGNAT (AprA residues 503–629) was subcloned from pAPS1 to create pMAS246. The region encoding AprA ACP (AprA residues 1058–1138) was subcloned from pAPS1 to create pAPS2. Plasmid pAPS3 was created by subcloning the sequence encoding GphF MT1-GNAT (GphF residues 2–696) from a partial *gphF* clone kindly provided by Richard Taylor (Notre Dame University) [18]. A GphF/H660A mutation was introduced (pMAS335) to block GphF GNAT decarboxylase activity. DNA sequencing was performed at the University of Michigan DNA Sequencing Core to verify all constructs and mutations. All constructs were recombinantly expressed in *Escherichia coli* and purified using nickel affinity and gel filtration chromatography.

Enzyme Assays

Acyl-ACPs were produced via incubation with acyl-CoAs and *Streptomyces verticillus* phosphopantetheinyl transferase (SVP). All assays were conducted in triplicate. 10 μL AprA methylation reaction mixtures containing 100 μM AprA acetyl-, isobutyryl-, malonyl-, methylmalonyl-, or propionyl-ACP were incubated with 25 μM wild type or mutagenized AprA MT1-ΨGNAT or AprA ΨGNAT, 1.35 mM SAM, and 0.5 mM $CaCl_2$, $CoCl_2$, $CuSO_4$, $(NH_4)_2Fe(SO_4)_2$, $NiSO_4$, $MgCl_2$, $MnCl_2$, Na_2MoO_4, or $ZnCl_2$, in 50 mM Hepes 7.4, 150 mM NaCl. For anaerobic reactions, all buffers were degassed through several freeze-pump-thaw cycles and brought into an anaerobic glove box. Solid $(NH_4)_2Fe(SO_4)_2$ and SAM, and aliquots of AprA MT1-ΨGNAT and ACP were preincubated for 1 hr in the anaerobic environment in a 0–4°C CoolBox prior to preparing Fe^{2+} and SAM solutions and reaction mixtures. Reactions were incubated 5 hr at 30°C (or 4 hr for the time course). AprA

acyltransfer reaction mixtures (10 μL) containing 100 μM AprA holo-ACP were incubated with 25 μM AprA ΨGNAT and 0.5 mM malonyl- or methylmalonyl-CoA in 50 mM Hepes 7.4, 150 mM NaCl. Reactions were incubated at 30°C for 10 hr. CurJ *C*-MT reaction mixtures (10 μL) containing 100 μM JamJ apo ACP, 25 μM CurJ *C*-MT, 10 μM SVP, 1 mM $MgCl_2$, 1.35 mM SAM, 0.5 mM $(NH_4)_2Fe(SO_4)_2$, and 0.5 mM malonyl-CoA in 50 mM Hepes 7.4, 150 mM NaCl. Reactions were incubated at 30°C for 5 hr. GphF reaction mixtures (10 μL) contained 100 μM AprA malonyl-ACP, 50 μM GphF MT1-GNAT H660A, 1.35 mM SAM, and 0.5 mM $(NH_4)_2Fe(SO_4)_2$ or $MnCl_2$, in 50 mM Hepes pH 7.4, 150 mM NaCl. Reactions were incubated at 20°C for 24 hr and quenched with 10% (v/v) formic acid prior to LC/MS analysis. Enzyme assays were slightly modified to assess AprA MT1-ΨGNAT activity on CoA substrates by monitoring absorbance at 254 nm of reaction mixtures separated by HPLC.

Protein Crystallization and Structure Determination

Crystal structures of AprA MT1-ΨGNAT were solved for a serendipitous double-substitution (S274I/Q528P) that was introduced during amplification of the gene and was essential to crystallization. The double substitution had no effect on catalytic activity. Native and SeMet AprA MT1-ΨGNAT/S274I/Q528P was crystallized by vapor diffusion in a 1:2 μL mixture of protein stock (10–11 mg mL^{-1} AprA MT1-ΨGNAT in Tris buffer C with 1 mM SAM) and well solution (2.4–2.5 M $(NH_4)_2SO_4$, 0.1 M Tris pH 8.5) at 4°C. Crystals were cryoprotected in 2.4 M $(NH_4)_2SO_4$ supplemented with 25% (v/v) glycerol and flash cooled in liquid nitrogen. Single-wavelength anomalous diffraction was used to determine the AprA MT1-ΨGNAT structure.

Mn-bound AprA MT1-ΨGNAT/S274I/Q528P was crystallized by vapor diffusion in a 2:1 μL mixture of protein stock (10–11 mg mL^{-1} of AprA MT1-GNAT in Tris buffer C with 1 mM SAM and 5 mM $MnCl_2$) and well solution (0.15 M DL-malic acid pH 7.0, 20% (w/v) PEG 3350) at 20°C. Malonate- and Mn-bound AprA MT1-ΨGNAT/S274I/Q528P was crystallized by vapor diffusion in a 1:1 μL mixture of protein stock (10–11 mg mL^{-1} AprA MT1-ΨGNAT in Tris buffer C with 1 mM SAM and 5 mM $MnCl_2$) and well solution (0.05 M sodium malonate, 16% (w/v) PEG 3350) at 4°C. A fully refined apo AprA MT1-ΨGNAT structure was used to solve the structure of Mn bound AprA MT1-ΨGNAT and Malonate- and Mn-bound AprA MT1-ΨGNAT.

Supplementary Material

Refer to Web version on PubMed Central for supplementary material.

Acknowledgments

We thank R. Taylor for the *gphF* DNA. This work was supported by National Institutes of Health (NIH) grants DK042303 to J.L.S.; CA108874 to D.H.S., W.H.G., L.G., and J.L.S.; and GM118101 to D.H.S. M.A.S. was supported by a predoctoral fellowships from an NIH Cellular Biotechnology Training Program (GM008353) and the University of Michigan Rackham Graduate School. A.P.S. was supported by a predoctoral fellowship from an NIH Molecular Biophysics Training Program (GM008270). N.A.M. was supported by a predoctoral fellowship from an NIH Marine Biotechnology Training Program (GM067550). GM/CA@APS is supported by the NIH National Institute of General Medical Sciences (AGM- 12006) and National Cancer Institute (ACB-12002).

References

1. Keatinge-Clay AT. The structures of type I polyketide synthases. Nat Prod Rep. 2012; 29:1050–1073. [PubMed: 22858605]
2. Ikeda H, Nonomiya T, Usami M, Ohta T, Omura S. Organization of the biosynthetic gene cluster for the polyketide anthelmintic macrolide avermectin in *Streptomyces avermitilis*. Proc Natl Acad Sci U S A. 1999; 96:9509–9514. [PubMed: 10449723]
3. Schwecke T, Aparicio JF, Molnar I, Konig A, Khaw LE, Haydock SF, Oliynyk M, Caffrey P, Cortes J, Lester JB, et al. The biosynthetic gene cluster for the polyketide immunosuppressant rapamycin. Proc Natl Acad Sci U S A. 1995; 92:7839–7843. [PubMed: 7644502]
4. Donadio S, Katz L. Organization of the enzymatic domains in the multifunctional polyketide synthase involved in erythromycin formation in *Saccharopolyspora erythraea*. Gene. 1992; 111:51–60. [PubMed: 1547954]
5. Keatinge-Clay AT. The Uncommon Enzymology of Cis-Acyltransferase Assembly Lines. Chem Rev. 2017; 117:5334–5366. [PubMed: 28394118]
6. Moore BS, Hertweck C. Biosynthesis and attachment of novel bacterial polyketide synthase starter units. Nat Prod Rep. 2002; 19:70–99. [PubMed: 11902441]
7. Cane DE, Liang TC, Kaplan L, Nallin MK, Schulman MD, Hensens OD, Douglas AW, G A-S. Biosynthetic Origin of the Carbon Skeleton and Oxygen Atoms of the Avermectins. J Am Chem Soc. 1983; 105:4110–4112.
8. Hafner EW, Holley BW, Holdom KS, Lee SE, Wax RG, Beck D, McArthur HA, Wernau WC. Branched-chain fatty acid requirement for avermectin production by a mutant of *Streptomyces avermitilis* lacking branched-chain 2-oxo acid dehydrogenase activity. J Antibiot (Tokyo). 1991; 44:349–356. [PubMed: 2026560]
9. Pulsawat N, Kitani S, Kinoshita H, Lee CK, Nihira T. Identification of the bkdAB gene cluster, a plausible source of the starter-unit for virginiamycin M production in *Streptomyces virginiae*. Arch Microbiol. 2007; 187:459–466. [PubMed: 17375285]
10. Silakowski B, Schairer HU, Ehret H, Kunze B, Weinig S, Nordsiek G, Brandt P, Blocker H, Hofle G, Beyer S, Muller R. New lessons for combinatorial biosynthesis from myxobacteria. The myxothiazol biosynthetic gene cluster of *Stigmatella aurantiaca* DW4/3-1. J Biol Chem. 1999; 274:37391–37399. [PubMed: 10601310]
11. Weinig S, Hecht HJ, Mahmud T, Muller R. Melithiazol biosynthesis: further insights into myxobacterial PKS/NRPS systems and evidence for a new subclass of methyl transferases. Chem Biol. 2003; 10:939–952. [PubMed: 14583260]
12. Pulsawat N, Kitani S, Nihira T. Characterization of biosynthetic gene cluster for the production of virginiamycin M, a streptogramin type A antibiotic, in *Streptomyces virginiae*. Gene. 2007; 393:31–42. [PubMed: 17350183]
13. Gu L, Geders TW, Wang B, Gerwick WH, Hakansson K, Smith JL, Sherman DH. GNAT-like strategy for polyketide chain initiation. Science. 2007; 318:970–974. [PubMed: 17991863]
14. Chang Z, Sitachitta N, Rossi JV, Roberts MA, Flatt PM, Jia J, Sherman DH, Gerwick WH. Biosynthetic pathway and gene cluster analysis of curacin A, an antitubulin natural product from the tropical marine cyanobacterium *Lyngbya majuscula*. J Nat Prod. 2004; 67:1356–1367. [PubMed: 15332855]
15. Favrot L, Blanchard JS, Vergnolle O. Bacterial GCN5-Related N-Acetyltransferases: From Resistance to Regulation. Biochemistry. 2016; 55:989–1002. [PubMed: 26818562]
16. Salah Ud-Din AI, Tikhomirova A, Roujeinikova A. Structure and Functional Diversity of GCN5-Related N-Acetyltransferases (GNAT). Int J Mol Sci. 2016; 17
17. Froese DS, Forouhar F, Tran TH, Vollmar M, Kim YS, Lew S, Neely H, Seetharaman J, Shen Y, Xiao R, Acton TB, Everett JK, Cannone G, Puranik S, Savitsky P, Krojer T, Pilka ES, Kiyani W, Lee WH, Marsden BD, von Delft F, Allerston CK, Spagnolo L, Gileadi O, Montelione GT, Oppermann U, Yue WW, Tong L. Crystal structures of malonyl-coenzyme A decarboxylase provide insights into its catalytic mechanism and disease-causing mutations. Structure. 2013; 21:1182–1192. [PubMed: 23791943]

18. Young J, Stevens DC, Carmichael R, Tan J, Rachid S, Boddy CN, Muller R, Taylor RE. Elucidation of gephyronic acid biosynthetic pathway revealed unexpected SAM-dependent methylations. J Nat Prod. 2013; 76:2269–2276. [PubMed: 24298873]
19. Kellmann R, Mihali TK, Jeon YJ, Pickford R, Pomati F, Neilan BA. Biosynthetic intermediate analysis and functional homology reveal a saxitoxin gene cluster in cyanobacteria. Appl Environ Microbiol. 2008; 74:4044–4053. [PubMed: 18487408]
20. Grindberg RV, Ishoey T, Brinza D, Esquenazi E, Coates RC, Liu WT, Gerwick L, Dorrestein PC, Pevzner P, Lasken R, Gerwick WH. Single cell genome amplification accelerates identification of the apratoxin biosynthetic pathway from a complex microbial assemblage. PLoS One. 2011; 6:e18565. [PubMed: 21533272]
21. Leao T, Castelao G, Korobeynikov A, Monroe EA, Podell S, Glukhov E, Allen EE, Gerwick WH, Gerwick L. Comparative genomics uncovers the prolific and distinctive metabolic potential of the cyanobacterial genus *Moorea*. Proc Natl Acad Sci U S A. 2017; 114:3198–3203. [PubMed: 28265051]
22. Huang KC, Chen Z, Jiang Y, Akare S, Kolber-Simonds D, Condon K, Agoulnik S, Tendyke K, Shen Y, Wu KM, Mathieu S, Choi HW, Zhu X, Shimizu H, Kotake Y, Gerwick WH, Uenaka T, Woodall-Jappe M, Nomoto K. Apratoxin A Shows Novel Pancreas-Targeting Activity through the Binding of Sec 61. Mol Cancer Ther. 2016; 15:1208–1216. [PubMed: 27196783]
23. Paatero AO, Kellosalo J, Dunyak BM, Almaliti J, Gestwicki JE, Gerwick WH, Taunton J, Paavilainen VO. Apratoxin Kills Cells by Direct Blockade of the Sec61 Protein Translocation Channel. Cell Chem Biol. 2016; 23:561–566. [PubMed: 27203376]
24. Simunovic V, Zapp J, Rachid S, Krug D, Meiser P, Muller R. Myxovirescin A biosynthesis is directed by hybrid polyketide synthases/nonribosomal peptide synthetase, 3-hydroxy-3-methylglutaryl-CoA synthases, and trans-acting acyltransferases. Chembiochem. 2006; 7:1206–1220. [PubMed: 16835859]
25. Sudek S, Lopanik NB, Waggoner LE, Hildebrand M, Anderson C, Liu H, Patel A, Sherman DH, Haygood MG. Identification of the putative bryostatin polyketide synthase gene cluster from "*Candidatus Endobugula sertula*", the uncultivated microbial symbiont of the marine bryozoan *Bugula neritina*. J Nat Prod. 2007; 70:67–74. [PubMed: 17253852]
26. Partida-Martinez LP, de Looss CF, Ishida K, Ishida M, Roth M, Buder K, Hertweck C. Rhizoxin, the first mycotoxin isolated from the zygomycota, is not a fungal metabolite but is produced by bacterial endosymbionts. Appl Environ Microbiol. 2007; 73:793–797. [PubMed: 17122400]
27. Kraft AS, Smith JB, Berkow RL. Bryostatin, an activator of the calcium phospholipid-dependent protein kinase, blocks phorbol ester-induced differentiation of human promyelocytic leukemia cells HL-60. Proc Natl Acad Sci U S A. 1986; 83:1334–1338. [PubMed: 3456591]
28. Skiba MA, Sikkema AP, Fiers WD, Gerwick WH, Sherman DH, Aldrich CC, Smith JL. Domain Organization and Active Site Architecture of a Polyketide Synthase *C*-methyltransferase. ACS Chem Biol. 2016; 11:3319–3327. [PubMed: 27723289]
29. Storm PA, Herbst DA, Maier T, Townsend CA. Functional and Structural Analysis of Programmed *C*-Methylation in the Biosynthesis of the Fungal Polyketide Citrinin. Cell Chem Biol. 2017; 24:316–325. [PubMed: 28238725]
30. Zou XW, Liu YC, Hsu NS, Huang CJ, Lyu SY, Chan HC, Chang CY, Yeh HW, Lin KH, Wu CJ, Tsai MD, Li TL. Structure and mechanism of a nonhaem-iron SAM-dependent *C*-methyltransferase and its engineering to a hydratase and an *O*-methyltransferase. Acta Crystallogr D Biol Crystallogr. 2014; 70:1549–1560. [PubMed: 24914966]
31. Meluzzi D, Zheng WH, Hensler M, Nizet V, Dorrestein PC. Top-down mass spectrometry on low-resolution instruments: characterization of phosphopantetheinylated carrier domains in polyketide and non-ribosomal biosynthetic pathways. Bioorg Med Chem Lett. 2008; 18:3107–3111. [PubMed: 18006314]
32. Dorrestein PC, Bumpus SB, Calderone CT, Garneau-Tsodikova S, Aron ZD, Straight PD, Kolter R, Walsh CT, Kelleher NL. Facile detection of acyl and peptidyl intermediates on thiotemplate carrier domains via phosphopantetheinyl elimination reactions during tandem mass spectrometry. Biochemistry. 2006; 45:12756–12766. [PubMed: 17042494]
33. Liscombe DK, Louie GV, Noel JP. Architectures, mechanisms and molecular evolution of natural product methyltransferases. Nat Prod Rep. 2012; 29:1238–1250. [PubMed: 22850796]

34. Bernard SM, Akey DL, Tripathi A, Park SR, Konwerski JR, Anzai Y, Li S, Kato F, Sherman DH, Smith JL. Structural basis of substrate specificity and regiochemistry in the MycF/TylF family of sugar *O*-methyltransferases. ACS Chem Biol. 2015; 10:1340–1351. [PubMed: 25692963]
35. Vidgren J, Svensson LA, Liljas A. Crystal structure of catechol *O*-methyltransferase. Nature. 1994; 368:354–358. [PubMed: 8127373]
36. Armstrong RN. Mechanistic diversity in a metalloenzyme superfamily. Biochemistry. 2000; 39:13625–13632. [PubMed: 11076500]
37. Hashimoto K, Suzuki H, Taniguchi K, Noguchi T, Yohda M, Odaka M. Catalytic mechanism of nitrile hydratase proposed by time-resolved X-ray crystallography using a novel substrate, tert-butylisonitrile. J Biol Chem. 2008; 283:36617–36623. [PubMed: 18948265]
38. Nagashima S, Nakasako M, Dohmae N, Tsujimura M, Takio K, Odaka M, Yohda M, Kamiya N, Endo I. Novel non-heme iron center of nitrile hydratase with a claw setting of oxygen atoms. Nat Struct Biol. 1998; 5:347–351. [PubMed: 9586994]
39. Arnett EM, Maroldo SG, Schilling SL, Harrelson JA. Ion pairing and reactivity of enolate anions. 5. Thermodynamics of ionization of β-di- and tricarbonyl compounds in dimethyl sulfoxide solution and ion pairing of their alkali salts. J Am Chem Soc. 1984; 106:6759–6767.
40. Poust S, Phelan RM, Deng K, Katz L, Petzold CJ, Keasling JD. Divergent mechanistic routes for the formation of gem-dimethyl groups in the biosynthesis of complex polyketides. Angew Chem Int Ed Engl. 2015; 54:2370–2373. [PubMed: 25564997]
41. Miller DA, Luo L, Hillson N, Keating TA, Walsh CT. Yersiniabactin synthetase: a four-protein assembly line producing the nonribosomal peptide/polyketide hybrid siderophore of Yersinia pestis. Chem Biol. 2002; 9:333–344. [PubMed: 11927258]
42. Mazur MT, Walsh CT, Kelleher NL. Site-specific observation of acyl intermediate processing in thiotemplate biosynthesis by fourier transform mass spectrometry: the polyketide module of yersiniabactin synthetase. Biochemistry. 2003; 42:13393–13400. [PubMed: 14621984]
43. Carreras CW, Khosla C. Purification and in vitro reconstitution of the essential protein components of an aromatic polyketide synthase. Biochemistry. 1998; 37:2084–2088. [PubMed: 9518007]
44. Florova G, Kazanina G, Reynolds KA. Enzymes involved in fatty acid and polyketide biosynthesis in *Streptomyces glaucescens*: role of FabH and FabD and their acyl carrier protein specificity. Biochemistry. 2002; 41:10462–10471. [PubMed: 12173933]
45. Ishikawa F, Sugimoto H, Kakeya H. In vitro investigation of crosstalk between fatty acid and polyketide synthases in the andrimid biosynthetic assembly line. Chembiochem. 2016; 17:2137–2142. [PubMed: 27598417]
46. Kampa A, Gagunashvili AN, Gulder TA, Morinaka BI, Daolio C, Godejohann M, Miao VP, Piel J, Andresson O. Metagenomic natural product discovery in lichen provides evidence for a family of biosynthetic pathways in diverse symbioses. Proc Natl Acad Sci U S A. 2013; 110:E3129–3137. [PubMed: 23898213]
47. Mattheus W, Gao LJ, Herdewijn P, Landuyt B, Verhaegen J, Masschelein J, Volckaert G, Lavigne R. Isolation and purification of a new kalimantacin/batumin-related polyketide antibiotic and elucidation of its biosynthesis gene cluster. Chem Biol. 2010; 17:149–159. [PubMed: 20189105]
48. Piel J. A polyketide synthase-peptide synthetase gene cluster from an uncultured bacterial symbiont of Paederus beetles. Proc Natl Acad Sci U S A. 2002; 99:14002–14007. [PubMed: 12381784]
49. Piel J, Hui D, Wen G, Butzke D, Platzer M, Fusetani N, Matsunaga S. Antitumor polyketide biosynthesis by an uncultivated bacterial symbiont of the marine sponge *Theonella swinhoei*. Proc Natl Acad Sci U S A. 2004; 101:16222–16227. [PubMed: 15520376]
50. Moebius N, Ross C, Scherlach K, Rohm B, Roth M, Hertweck C. Biosynthesis of the respiratory toxin bongkrekic acid in the pathogenic bacterium *Burkholderia gladioli*. Chem Biol. 2012; 19:1164–1174. [PubMed: 22999884]
51. Stols L, Gu M, Dieckman L, Raffen R, Collart FR, Donnelly MI. A new vector for high-throughput, ligation-independent cloning encoding a tobacco etch virus protease cleavage site. Protein Expr Purif. 2002; 25:8–15. [PubMed: 12071693]

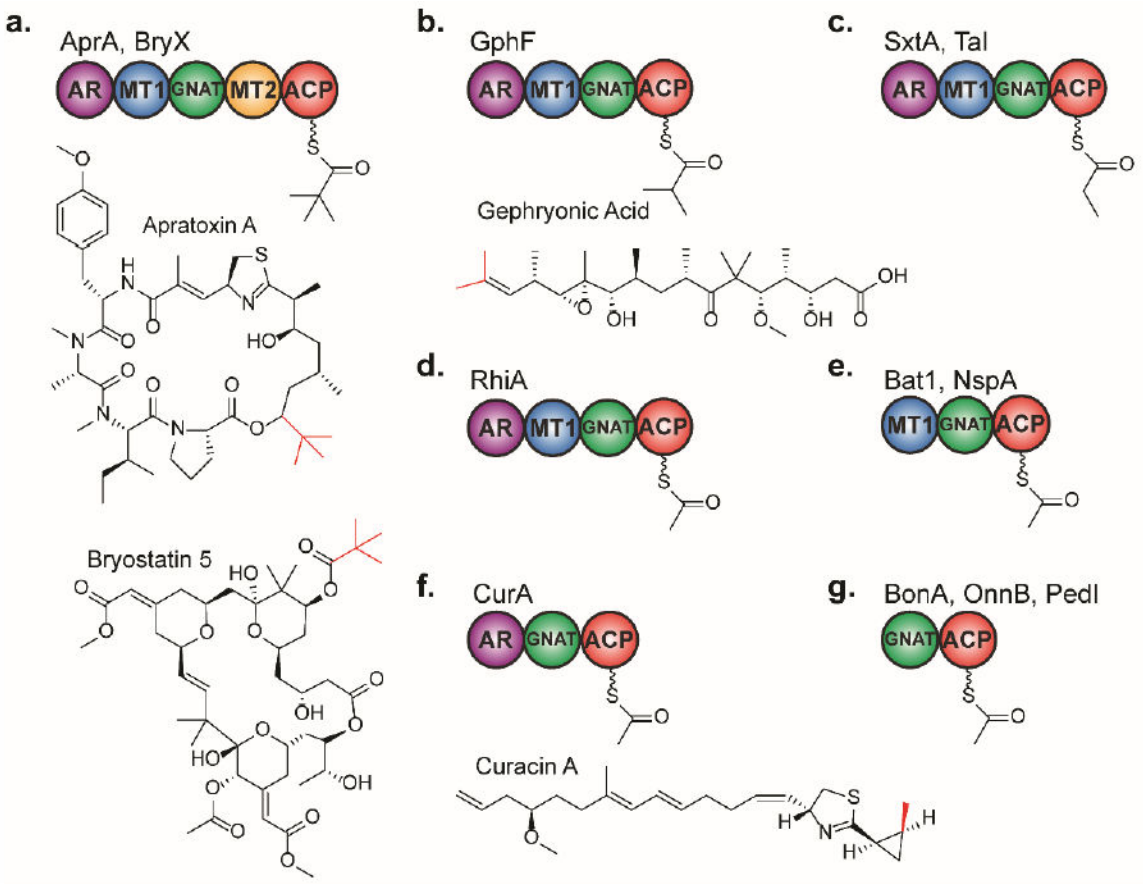

Figure 1.

Domain architecture of GNAT loading modules: Adaptor region (AR), methyltransferase (MT), GCN5-related *N*-acetyltransferase (GNAT), acyl carrier protein (ACP). Starter units produced by GNAT loading modules in select metabolites are colored in red. Pathway abbreviations are as follows: Apr- apratoxin A, Bry- bryostatin, Gph- gephyronic acid, Sxt- saxitoxin, Ta- myxovirescin A, Rhi- rhizoxin, Bat- batumin, Nsp- nosperin, Cur- curacin A, Bon- bongkrekic acid, Onn- onnamide, Ped- pederin.

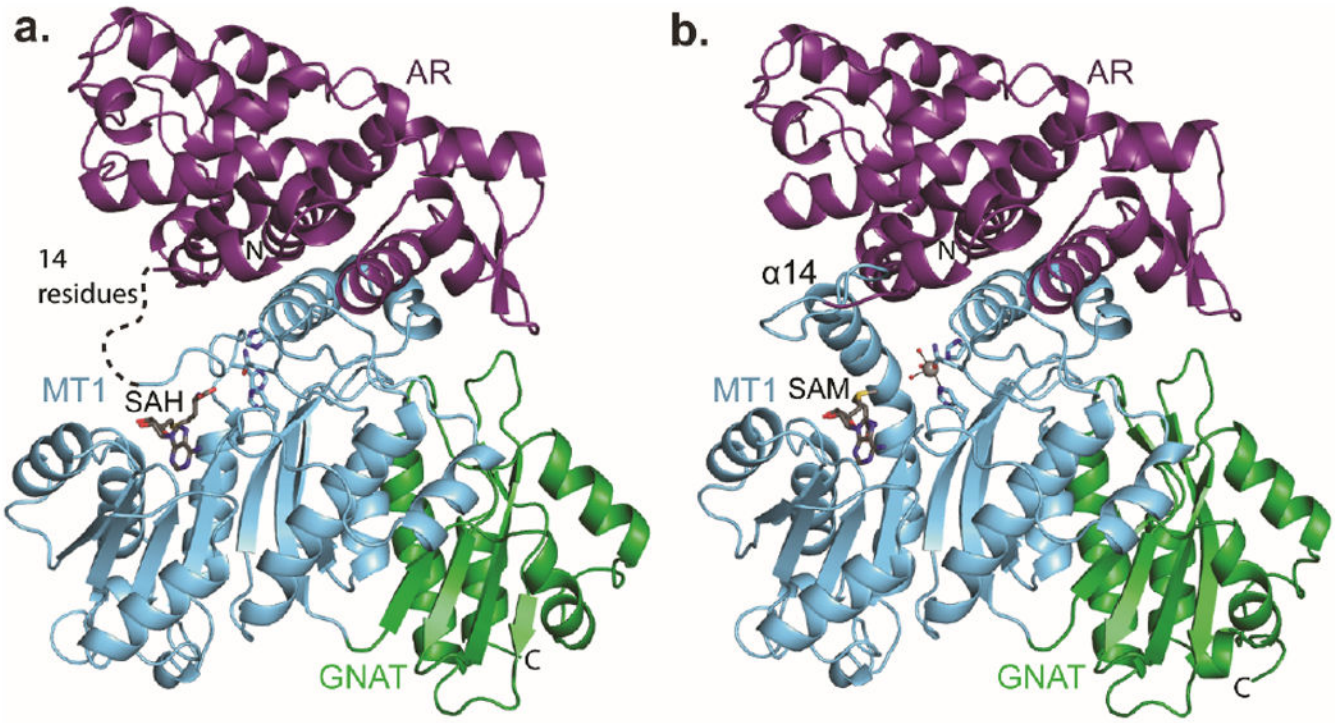

Figure 2.

Structures of AprA AR-MT1-YGNAT colored by structural region (AR, purple; MT1, blue; ΨGNAT, green). SAH or SAM is shown in sticks with atomic colors (C, gray; O, red; N, blue; S, yellow). Disordered residues in the lid-core connector (228–240) are indicated with a dashed line. a) AprA AR-MT1-ΨGNAT. b) AprA AR-MT1-ΨGNAT with bound Mn^{2+}. Mn is shown as a gray sphere and water ligands as red spheres.

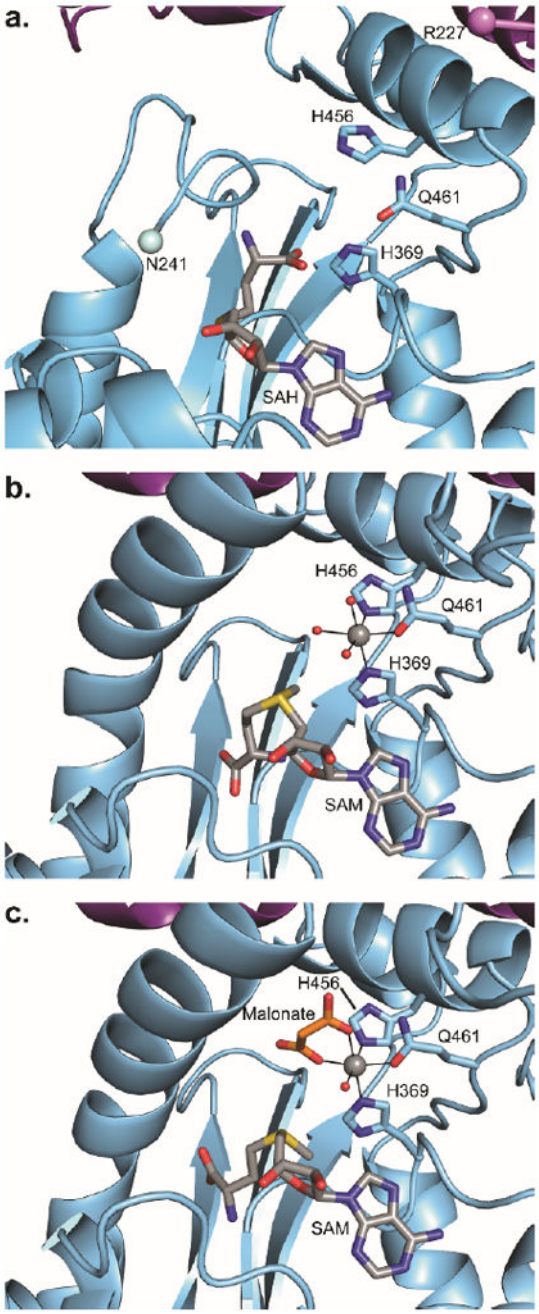

Figure 3.

AprA MT1 active sites. a) Metal-free AprA MT1-ΨGNAT with SAH. Arg227 before and Asn241 after the disordered lid-core linker are designated with spheres. b) AprA MT1-ΨGNAT with Mn^{2+} and SAM. c) AprA MT1-ΨGNAT substrate complex with Mn^{2+}, malonate and SAM. MT1 structural regions are colored as in Figure 2. Mn^{2+} (gray) and water ligands (red) are shown as spheres. Mn^{2+} ligands (blue C), SAH/SAM (gray C), and malonate (orange C) are shown in sticks with atomic colors.

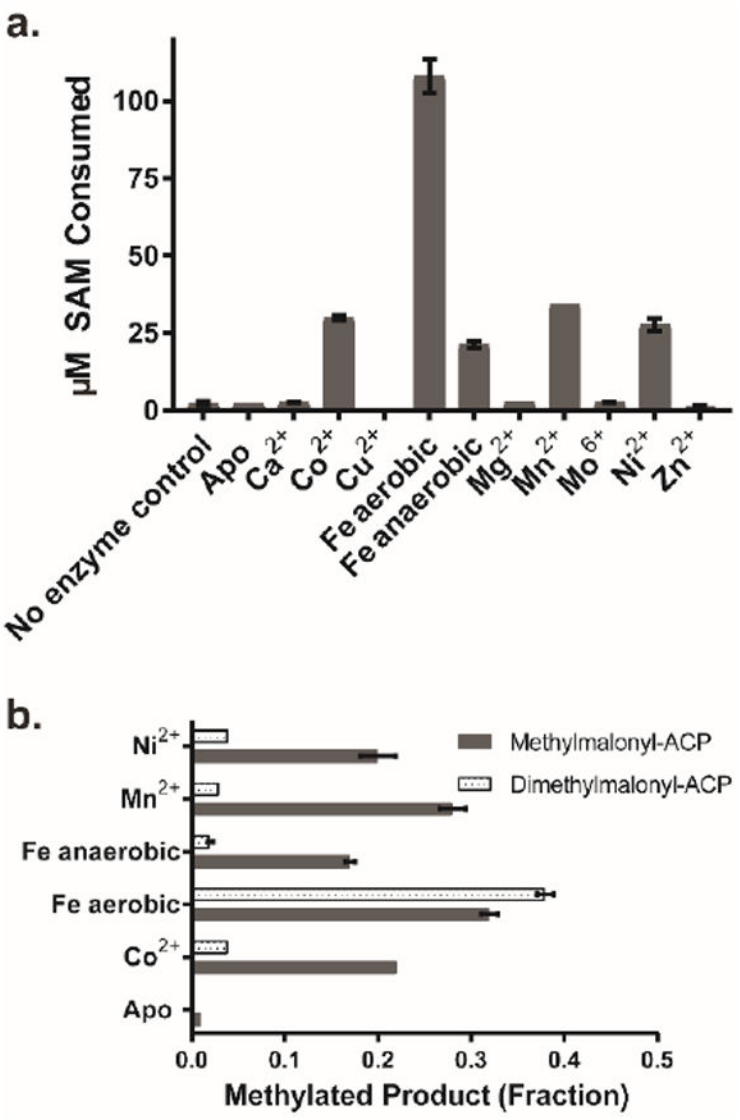

Figure 4.

AprA MT1-ΨGNAT activity. a) Metal profile of reactions with malonyl-ACP. The percent of Ppant ejection fragments from methylmalonyl- and dimethylmalonyl-ACP are represented as equivalents of SAM consumed. b) Ratios of methylmalonyl-ACP and dimethylmalonyl-ACP products of the reactions in a. Error bars represent triplicate experiments and, in some cases, are too small to be visible.

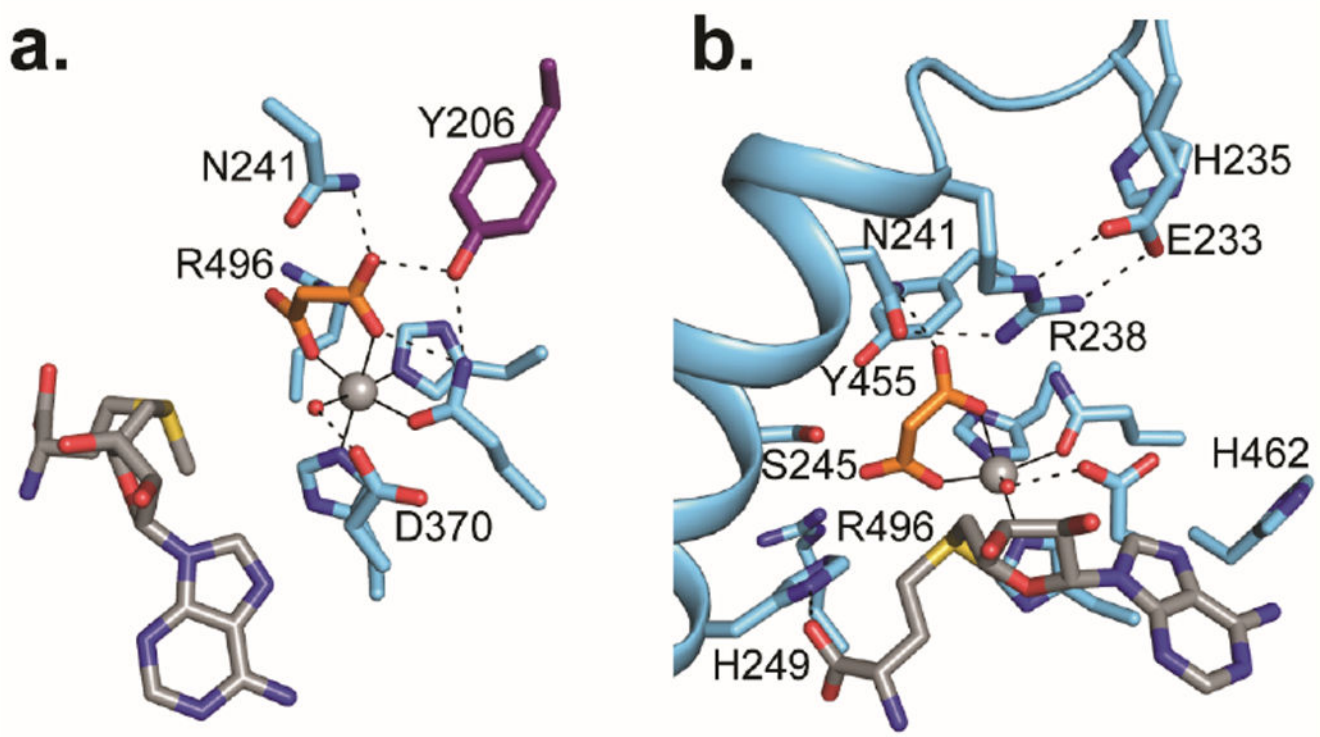

Figure 5.

Key amino acids for substrate binding. (A) Malonate interactions at the metal center. (B) Hydrogen bond network in lid-core connector (amino acids 228–251). Amino acid side chains (purple C, blue C), SAM (gray C), and malonate (orange C) are shown in sticks with atomic coloring, hydrogen bonds as dashed lines, and metal coordination bonds as solid lines.

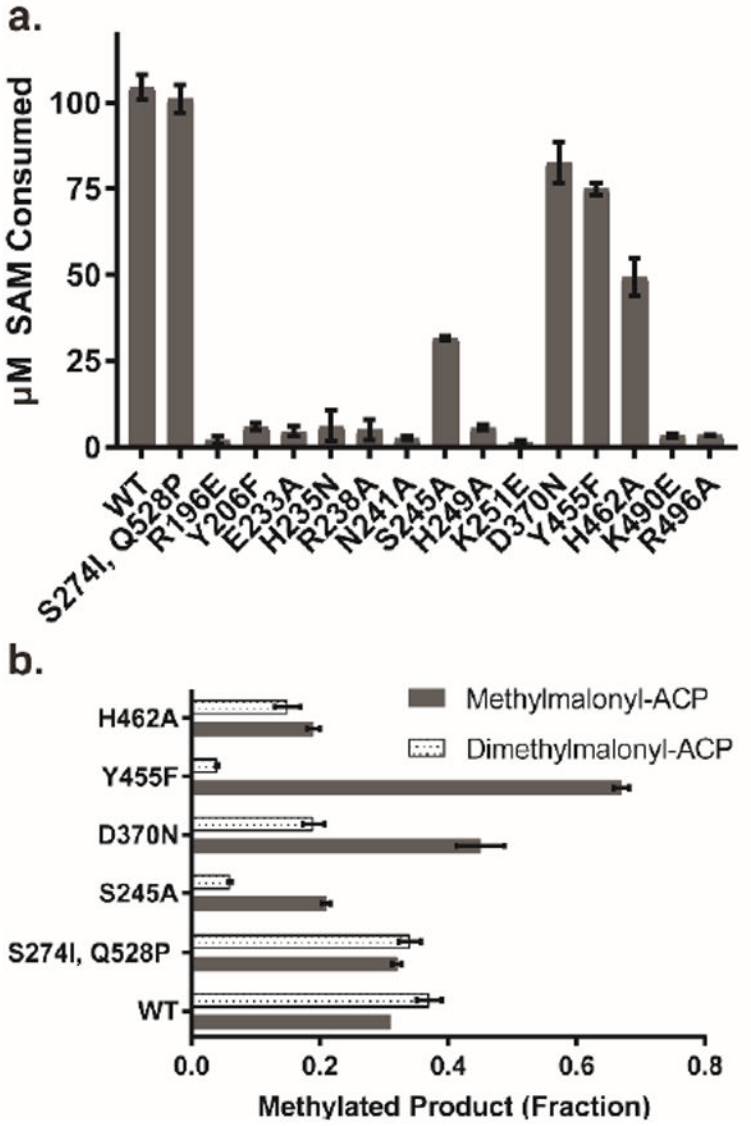

Figure 6.

Relative methylation activities of wild type AprA MT1-ΨGNAT, serendipitous crystallization substitution (S274I/Q528P), and active site variants. a) SAM consumption in reactions with malonyl-ACP. b) Ratios of methylmalonyl-ACP and dimethylmalonyl-ACP products from a. Error bars represent triplicate experiments and, in some cases, are too small to be visible.

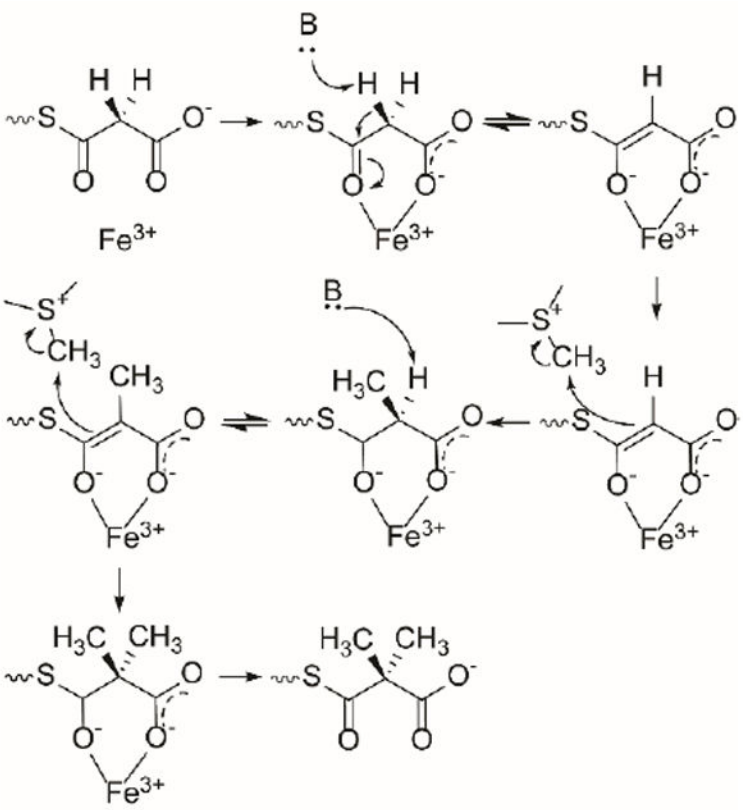

Figure 7.

AprA MT1 mechanism. Fe^{3+} acts as a Lewis acid to promote methylation at the α-carbon of malonyl-ACP to produce (*S*)-methylmalonyl-CoA. Methylmalonyl-ACP is subsequently methylated to dimethylmalonyl-ACP.

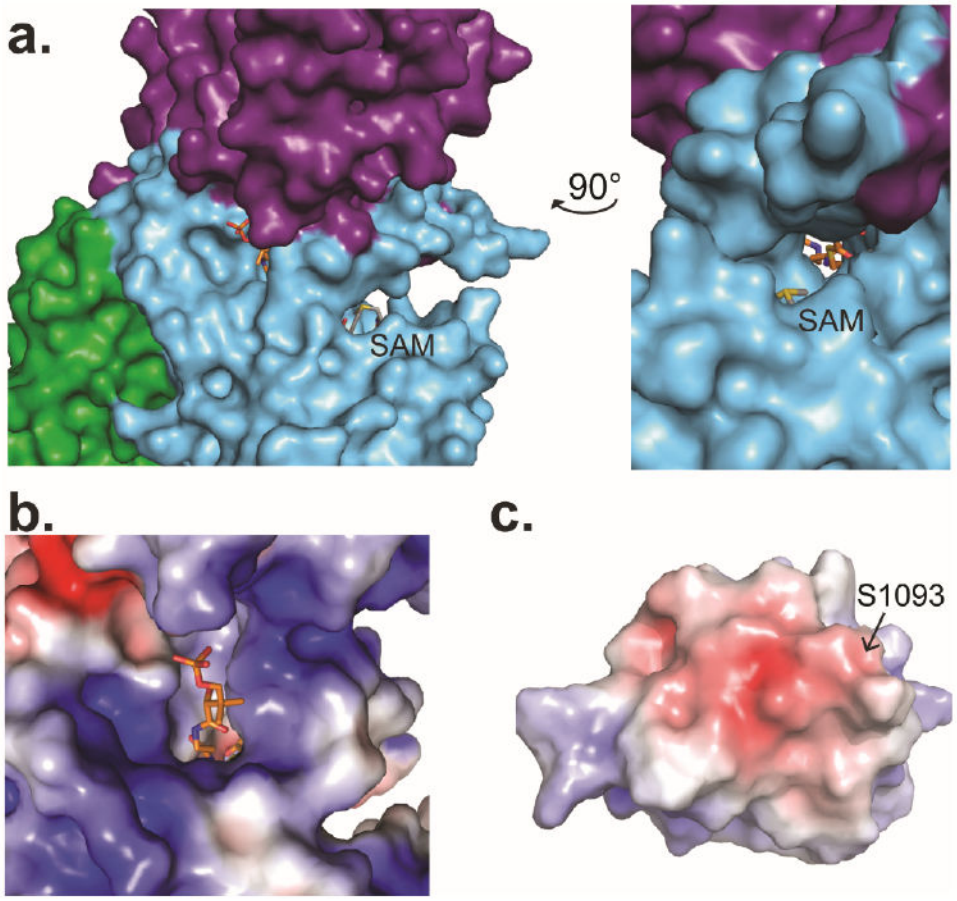

Figure 8.

Malonyl-Ppant substrate modeling. a) MT1-ΨGNAT surface showing Ppant, SAM and the tunnel created by active site assembly. Ppant (orange C) and SAM (gray C) are shown in sticks. Modeled malonyl-Ppant spans tunnel between the MT1 lid (purple) and core (blue). SAH can exchange with SAM while the substrate is still bound in the active site. b) Electrostatic surface of AprA c) Electrostatic surface of homology model of AprA GNAT. Ser1093 is the Ppant attachment site. Electrostatic surfaces shown at 5 kT/e, blue electropositive, red electronegative.